CHAPTER 5

Comparison of non-catalytic and in-situ catalytic pyrolysis of *Melia azedarach* sawdust

Abstract

This study focused on the in-situ catalytic pyrolysis of *Melia azedarach* sawdust by impregnating it with copper (Cu). Native and Cu impregnated *Melia azedarach* sawdust (MAS-N and MAS-C, respectively) were subjected to pyrolysis. MAS-N and MAS-C were characterized using proximate, ultimate and HHV analysis. Thermal degradation performance of MAS-N and MAS-C were examined by thermogravimetric analysis. Similar shapes of thermogravimetric curves indicated that Cu metal did not alter degradation pathway but lowered decomposition temperature and higher reaction rates were noticed for MAS-C due to catalytic effect of Cu. Optimization of operating process parameters was done by varying temperature, sweeping gas flow rate, particle size, packed bed height, pyrolysis time and heating rate for MAS-N. Maximum bio-oil yield for MAS-N was obtained at 550 ℃ temperature, 150 mL/min nitrogen flow rate, 8.4 cm bed height, 0.18-0.29 mm sized particles, 20 ℃/min heating rate and 60 min pyrolysis time. Further, effect of variation in temperature and catalyst to biomass ratio was studied for MAS-C and maximum bio-oil yield for MAS-C was obtained at lower temperature than that for MAS-N.

Results were compared for catalytic and non-catalytic pyrolysis products via various characterization methods. Bio-oil properties were analysed by FTIR, GC-MS and ^{13}C NMR. Proximate, ultimate, HHV, FTIR, XRD, SEM and BET surface area analysis were

used to characterize properties of bio-char. Results suggested that Cu has catalytic effect on pyrolysis products. This article will be useful for promoting future research related to using heavy metal contaminated biomass as potential opportunities.

5.1 Introduction

Fossil-based energy is exhaustible and accompanied by adverse impacts at local, regional, and global levels for environment, ecology, human beings and flora and fauna (Valizadeh et al., 2022). Climatic conditions of the planet are being burdened due to population growth (Gautam and Mondal, 2023a; Gautam and Mondal, 2023b). Hike of world population will strain on the environmental resources. Generating energy from waste biomass is a sustainable, novel and renewable green-energy generation approach for addressing energy-linked environmental impacts focusing on generation of wealth-from-waste (Valizadeh et al., 2022; Kim et al., 2022).

Pyrolysis is a thermochemical route for transforming biomass into biofuels (pyrolysis liquid called as bio-oil, solid bio-char and gases) at high temperature and inert atmospheric conditions (Yang et al., 2022). Bio-oil has several drawbacks like high oxygen content, ignition delay, high acidity and viscosity which create limitations of pyrolysis-to-energy chain (Buyang et al., 2023). Different catalysts have been reported to be employed to upgrade the bio-oil (Agnihotri and Mondal, 2022). Using commercial catalysts makes pyrolysis costly. Thus, some renewable and low-cost catalyst is required. In literature many pyrolysis studies using metal catalysts have been reported, for example TiO_2 based catalysts for corn straw (Dong et al., 2019), high-entropy alloy composed of Mn, Fe, Co, Ni, and Cu for upcycling of abandoned banners (Park et al., 2019), Cu/Al_2O_3 catalyst for tomato waste (Ozbay et al., 2018), metal-modified HZSM5 for wheat straw (Shao et al., 2019), and valorization of heavy metals-containing livestock manure into

biochar catalysts (Zeng et al., 2022). Heavy-metal-polluted biomass is often seen as nuisances but using it for pyrolysis can give catalytic effect due to rich metal content in it. The heavy-metal-polluted biomass is generated from heavy metal biosorption process or phytoremediation of metal polluted water bodies, abandoned mines, and even activated sludge. Han et al. (2018) impregnated *Arundo donax* and *Broussonetia papyrifera* with cadmium (Cd), copper (Cu) and lead (Pb) and reported that heavy metals imparted their catalytic effect and reduced the activation energy of pyrolysis (Han et al., 2018). He et al. (2019a) found that heavy metal contaminated *Avicennia marina* biomass produced hydrocarbon rich bio-oil as compared to that produced by uncontaminated biomass (He et al., 2019a). Koppolu et al (2004) investigated Zn, Ni, Cu, Co and Cr contaminated biomasses and found that metals increased the yield of condensable products (Koppolu et al., 2004).

However, due to diversified practical uses heavy metals could get incorporated into the biomass at trace to high concentration levels (Zhang et al., 2023). Phytoremediation, prolonged use of chemical fertilizers, industrial effluents and heavy metal adsorption onto biomass are prime sources of heavy metal contaminated biomass (He et al., 2021). Amongst various disposal methods like incineration, pyrolysis and gasification for heavy metal contaminated biomass, pyrolysis is emerging as a promising thermochemical route for mitigating environmental risks, value-added bio-fuel production and heavy-metal recovery (Han et al., 2018; Chai et al., 2022) Metals (Cu, Zn, Cd, Pb, Ni, and Cr etc.) are enriched in biochar during pyrolysis, thus metal-free bio-oil is obtained (Raheem et al., 2022). Heavy metal loaded biomass derived photocatalysts possess low bandgap energy (Chen et al., 2019). Therefore, in biomass heavy metals may impart synergistic effects by acting as a catalyst (Chai et al., 2022a).

The reported studies in literature are a good start for producing high-value chemicals from heavy-metal loaded biomass, but still enormous research blanks are there for converting heavy metal contaminated waste biomass into high value-added chemicals. Detailed evaluation is important for potential and effective utilization and value addition to contaminated biomass via pyrolysis. Also, no study using copper (Cu) as catalyst for *Melia azedarach* sawdust in in-situ mode is reported till now. The Key objectives of this study are (1) to use copper (Cu) as a catalyst and carry out catalytic and non-catalytic pyrolysis of *Melia azedarach* sawdust (MAS) and evaluate the influence of Cu impregnation on MAS. Cu is a common heavy-metal and found in effluent of industries like electroplating industry. (2) to elucidate the pyrolysis characteristics of catalytic and non-catalytic MAS, using thermal gravimetric analysis (TGA). (3) in-depth characterization of catalytic and non-catalytic bio-oil and bio-char by standard characterization techniques. Bio-oil properties were analysed by FTIR, GC-MS and ^{13}C NMR analysis. Bio-char was characterized for its physical and chemical properties by using proximate, ultimate, HHV, FTIR, XRD, SEM and BET surface area analysis. This study would provide a new pathway for simultaneous management of the waste biomass and the heavy metal pollution.

5.2 Material and methods

5.2.1 Collection of raw material and its preparation

Melia azedarach sawdust (MAS-N) utilized in this study was obtained from a lumber mill situated in the vicinity of campus of IIT-BHU Varanasi (25.3176° N, 82.9739° E), Uttar Pradesh, India. MAS was washed with plenty of tap-water and cleansed with distilled water. Then, it was sundried for 60 h (as per weather conditions) followed by incubating in oven at 105 ℃ until constant sample mass was attained. This MAS sample was further

pulverized and sieved to get particles of size range 0.18-0.29 mm by passing it through mesh no. 48 and retaining on mesh no. 80 along with particles of other size range. These samples were stored in air-tight glass containers and kept inside desiccators for utilization in experimental runs.

5.2.2 Catalyst and sample preparation

Synthetic waste water was prepared at lab scale by using analytical grade metal salt (procured from Thermo Fisher Scientific India Pvt. Ltd.). Specific quantity of $Cu(NO_3)_2 \cdot 3H_2O$ (Copper nitrate trihydrate) salt was dissolved in deionized water. Then, MAS-N was blended with the prepared waste water in the ratio of 1:10, 1:15 and 1:20 (gm/ml) at 100 ℃ over a magnetic stirrer (IKA Magnetic Stirrers RT 5) until water was completely evaporated, further it was dried in oven at 105 ℃ overnight to obtain heavy metal doped catalytic samples. Finally, it was sieved to an ideal particle size of 0.18-0.29 mm and named as MAS-C.

5.2.3 Pyrolysis experiments and characterization techniques

Non-catalytic bio-oil and bio-char (produced from MAS-N) were named as BO-N and BC-N, respectively while catalytic bio-oil and bio-char as BO-C and BC-C. Pyrolysis experiments and characterization techniques were similar as already described in section 4.2. For catalytic pyrolysis study MAS-C samples were used.

5.3 Results and discussion

5.3.1 Optimization of operating process parameters

Prominent parameters that influence pyrolysis product distribution are temperature, sweeping gas flow rate, particle size, packed bed height, pyrolysis time and heating rate. So, these parameters were explored in this study. Prior to catalytic pyrolysis operating

process parameters were optimized for non-catalytic biomass (MAS-N) pyrolysis. For investigating influence of temperature on pyrolytic product yield of MAS-N 450, 500, 550 and 600 ℃ were chosen and the same has been illustrated by Fig. 5.1a. These values of temperature were chosen based on TGA results and data available for various biomass in the existing literature. Bio-oil yield increased as temperature was increased and highest bio-oil yield of 50.6 (±1.03) wt.% was obtained at 550 ℃ and beyond this temperature bio-oil and bio-char yield decreased but gaseous yield increased owing to the fact that char and pyrolytic gases transformed into gaseous phase via secondary cracking and rapid endothermic degradation of biomass (Park et al., 2008).

Influence of sweeping gas flow rate on MAS-N pyrolytic end products was optimized using nitrogen flow rate of 100, 150 and 200 mL/min and as depicted in Fig. 5.1b. Maximum bio-oil yield (50.6 (±1.03) wt.%) was attained at 150 mL/min flow rate of N_2. At 150 mL/min pyrolytic vapours get sufficient retention time inside the reactor as well as in condensation zone which facilitates enhanced secondary cracking reactions leading to high bio-oil yield (Guedes et al., 2018). In order to probe influence of particle size on pyrolytic end product yield distribution, particles of three size range namely, mesh no. 80, 48, 32 and 20 which have size 0.18-0.29, 0.29-0.49 and 0.49-0.83 mm were used. It is worth noticing from Fig. 5.1c that small sized particles produce more bio-oil as heat transfer at high rate occurs in them which leads to efficient biomass devolatilization. Whereas, in large particles more bio-char formation occurs due to vapours formed as a result of thermal cracking have to cover more distance of char layer that promotes secondary reactions (Casoni et al., 2015). Packed bed height parameter was optimized by varying it from 8.4 to 2.1 cm and optimum bio-oil yield was achieved at 8.4 cm bed height and same is represented graphically in Fig. 5.1d. Enhancement in bio-oil yield with increasing height of bed could be attributed to the fact that increased bed height prevents

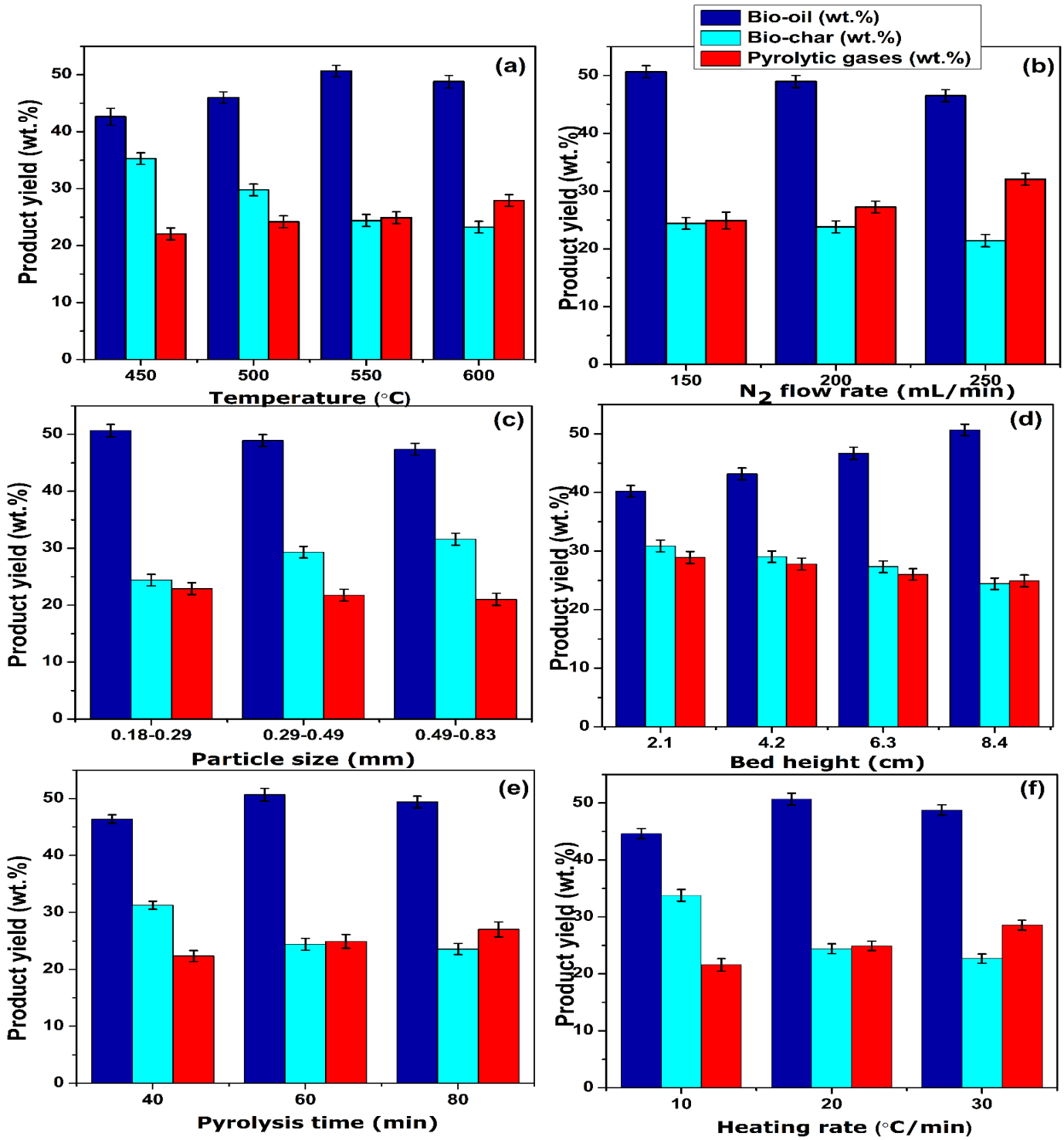

Figure 5.1. Effect of (a) temperature (b) N_2 flow rate (c) particle size (d) bed height (e) pyrolysis time and (f) heating rate on pyrolysis product yield of MAS-N. (550 °C temperature, 150 mL/min N_2 flow rate, 0.18-0.29 mm particles, 8.4 cm bed height, 60 min pyrolysis time and 20 °C/min heating rate unless stated their variation)

early escape of condensable volatile vapours and longer residence time in reaction zone leads to cracking of primary organic vapours along with accelerated secondary cracking of organic matter. Similar results were reported by Tripathi et al. (2016) in their study (Tripathi et al., 2016).

Effect of pyrolysis time on MAS-N pyrolytic product distribution was evaluated at 40, 60 and 80 min pyrolysis residence time within the reactor. It is worth noticing from Fig. 5.1e that the maximum bio-oil yield of 50.6 (±1.03) wt.% was attained for 60 min residence time and it got reduced by 2.5 wt.% when pyrolysis time was further elevated to 80 min. Pyrolytic gaseous yield enhanced with increasing pyrolysis time owing to the fact that prolonged pyrolytic residence time accelerated gasification of primary pyrolysis vapours and bio-char devolatilization because of secondary thermal degradation reactions. Similar findings were announced for Crofton weed (Cheng et al., 2019), pistachio shell (Acıkalın et al., 2012), and sawdust of furniture waste (Uzun et al., 2013). To examine the governing behaviour of heating rate on MAS-N pyrolytic product distribution, three heating rates 10, 20 and 30 ℃/min were employed. It is clearly evident from Fig. 5.1f that bio-oil's yield improved from 44.6 (±0.88) to 50.6 (±1.03) wt.% as heating rate was increased from 10 to 20 ℃/min but at 30 ℃/min it diminished owing to the fact that heating rate higher than optimum value gives rise to swift depolymerization of biomass into primary volatiles along with accelerated secondary reactions in pyrolytic vapours. Yield of bio-char declined but pyrolytic gaseous products yield enhanced with increasing heating rate. This decline in yield of bio-char with increase in the pyrolysis heating rate could be due to the fast and significant primary decomposition of MAS-N and secondary decomposition of the char residue. In fact, higher heating rates reduced limitations of heat and mass transfer which resulted in higher oil yields (Apaydin-Varol et al., 2014). Similar findings have been reported for Samanea saman seeds (Mishra et al., 2020), *Zea mays*

(Demiral et al., 2012), and alligator weed (Bhattacharjee and Biswas, 2019) in the literature.

Optimum operating parameters for pyrolysis of MAS-N pyrolysis were found to be 550 ℃ temperature, 150 mL/min nitrogen flow rate, 8.4 cm bed height and particle size in the range of 0.18-0.29 mm at a heating rate of 20 ℃/min coupled with 60 min pyrolysis time. Bio-oil yield was 50.6 (±1.03) wt.%, and bio-char and gas yield were 24.4 (±1.06) and 24.9 (±1.05) wt.%, respectively. Highest quantity of bio-oil was produced corresponding to these values of operating parameters. These selected values of temperature, nitrogen purging rate, bed height, size of particle, pyrolysis time and heating rate provided adequate heat and mass transfer for breakdown of MAS-N into condensable volatile hydrocarbon compounds inhibiting over breakdown of MAS-N into gaseous products.

5.3.2 Effect of biomass to catalyst ratio on pyrolytic products' yield

Role of catalyst is crucial for enhancement of targeted value-added products via pyrolysis. Optimization of feed to catalyst ratio becomes important for pyrolysis experiments for obtaining robust results. The effect of ratio of MAS-N to catalyst was studied and the same has been presented graphically in Fig. 5.2. Biomass (MAS-N) to catalyst ratio of 1:10, 1:15 and 1:20 (gm/mL) were considered in this study. Quantity of MAS-N (0.18-0.29 mm particle size) was kept constant (20g) and quantity of wastewater was varied to get MAS-C samples with different biomass to catalyst ratio. Sweeping gas was purged at a flow rate of 150 mL/min and pyrolysis temperature was kept at 500 ℃. It can be clearly observed from the Fig. 5.2 that bio-oil yield increased on increasing MAS to catalyst ratio from 1:10 (49.1 wt.%) to 1:15 (51.3 wt.%) but it decreased when ratio was further increased to 1:20 (49.2 wt.%). This is due to elevated heat transfer rate in impregnated MAS-C provided by Cu catalyst but upon further increasing catalyst quantity secondary cracking and repolymerization increased which resulted in bio-oil

yield decrement and increased bio-char yield. These results are in good harmony with that reported for copper impregnated fir sawdust (Liu et al., 2012). So, a biomass to catalyst ratio of 1:15 was found to be optimum and it was used in further experimental runs.

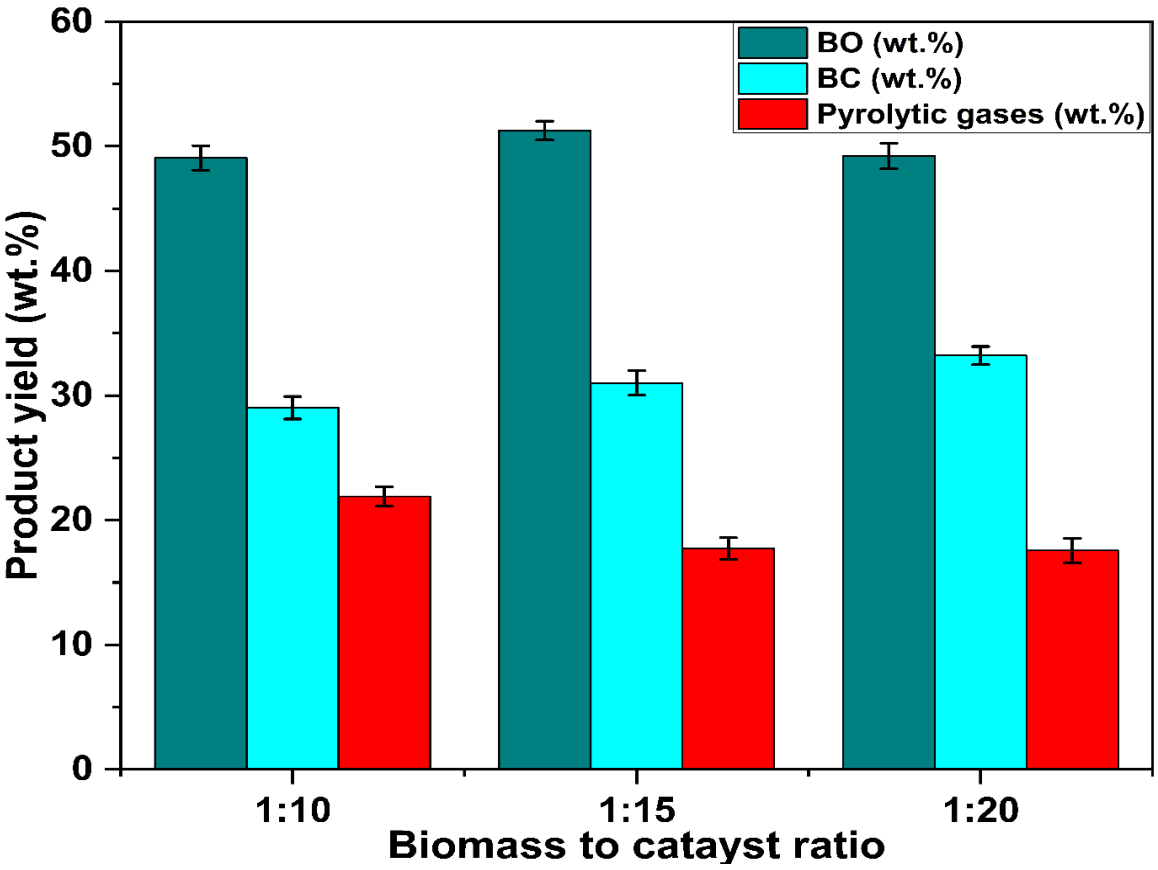

Figure 5.2. Effect of biomass to catalyst ratio on catalytic pyrolysis product yield distribution (Frozen parameters; 500 ℃ temperature, 150 mL/min N_2 flow rate, 0.18-0.29 mm particles, 8.4 cm bed height, 60 min pyrolysis time and 20 ℃/min heating rate)

5.3.3 Effect of temperature on catalytic pyrolysis

As per the findings of operating parameters' optimization study of MAS-N in section 5.3.1, of all the parameters temperature was found to be the parameter of utmost importance as it affected product yield distribution of pyrolysis the most. Variation in all

other parameters affected product yield barely, so effect of temperature variation on MAS-C pyrolytic product yield distribution was assessed. Fig. 5.3 displays the effect of temperature variation on pyrolytic products' yield of MAS-N and MAS-C. Catalytic pyrolysis was carried at 450, 500, 550 and 600 ℃ and results were compared with that obtained for MAS-N. Other operating parameters were kept at optimum values as obtained in section 5.3.1, that is, 150 mL/min nitrogen flow rate, 8.4 cm bed height and particle size in the range of 0.18-0.29 mm at a heating rate of 20 ℃/min at 60 min pyrolysis time. Pyrolytic bio-oil yield increased with increasing temperature for both MAS-N and MAS-C but after reaching optimum value it started declining. Maximum bio-oil yield of 51.3 wt.% for MAS-C was obtained at 500 ℃ while that for MAS-N was 50.6 wt.% at 550 ℃. Similarly, at all temperature pyrolytic liquid yield was more for MAS-C as compared with MAS-N. This indicated that use of Cu in MAS-C as catalyst improved bio-oil yield and due to catalytic effect of Cu metal maximum yield was obtained at lower temperature as compared to MAS-N. Lui et. al. (2011) also reported that yield of bio-oil for fir sawdust improved at all the temperatures upon carrying out in-situ catalytic pyrolysis by impregnating it with copper (Lui et. al., 2011). Similarly, it was reported that upon impregnating *Arundo donax* and *Broussonetia papyrifera* with heavy metals, pyrolysis activation energy reduced which in turn promoted the pyrolysis (Han et al., 2018). Similar results were reported for poplar wood upon impregnation (Hwang et al., 2013).

Catalytic and non-catalytic bio-oils obtained at optimum conditions were analysed for their water content and it was found to be 30.7 wt.% and 29.4 wt.%, respectively. Similar results were reported for tomato waste as its water content changed 11.33 to 10.74 wt.% upon impregnating it with metal (Ozbay et al., 2018).

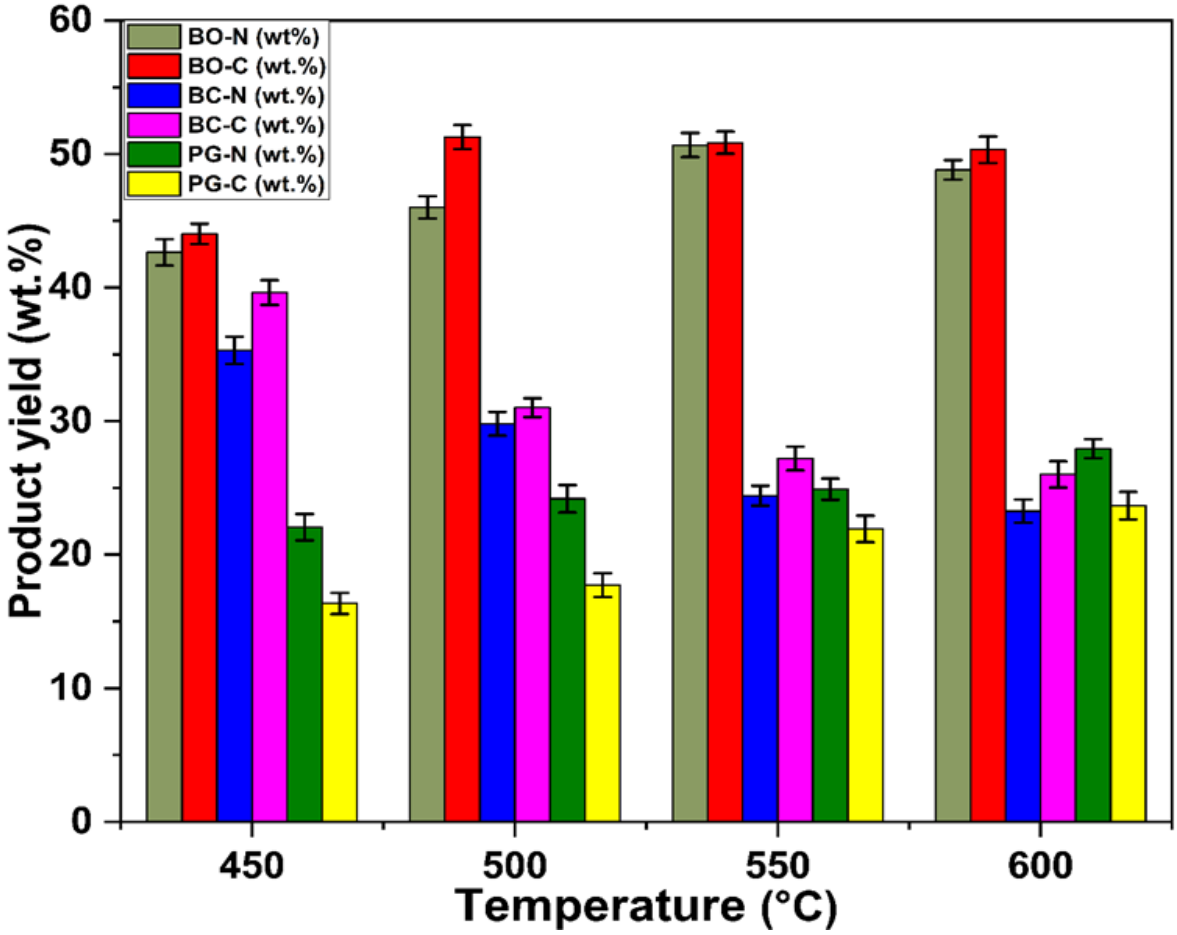

Figure 5.3. Variation in pyrolysis product yield of MAS-N and MAS-C with temperature (Frozen parameters; 150 mL/min N_2 flow rate, 0.18-0.29 mm particles, 8.4 cm bed height, 60 min pyrolysis time and 20 ℃/min heating rate)

5.3.4 Characterization of biomass and bio-char

The findings of proximate, ultimate and HHV analysis of MAS-N, MAS-C and their bio-chars are presented in Table 5.1. Raw substrate and bio-char exhibited different properties. MAS-N and MAS-C both are rich in volatile matter (78.30 and 78.1 wt.% respectively) meanwhile moisture and ash content in them is low. Biomass materials which possess less ash and moisture content (< 10 wt.%) along with high volatile matter are favourable for pyrolysis. High volatile matter containing feedstocks result in high bio-oil yields (Agnihotri and Mondal, 2023b). Presence of high fixed carbon content in them

is also advantageous for energy generation. Less nitrogen and sulfur content in MAS-N and MAS-C make them safe and environment-friendly. HHV of MAS-N (16.34 MJ/kg) makes it suitable for bioenergy generation. Volatile matter decreased in BC-N (32.1 wt.%) and when pyrolysis of MAS-C was carried out at 450, 500, 550 and 600 ℃ bio-char's volatile matter content decreased from 31.7 to 22.1 wt.% owing to the fact that volatiles present in biomass underwent conversion on being subjected to pyrolysis. Volatile matter in biochar of MAS-C was less as compared to biochar produced by MAS-N (i.e., BC-N) because catalytic effect of Cu facilitated much more release of volatiles. Ash and fixed carbon content of biochar increased. Increase in ash content of catalytic bio-char could be attributed to the presence of impregnated Cu metal in them.

Outcomes of elemental analysis of biomass and bio-char revealed higher content of oxygen in biomass as compared to bio-char (Table 5.1). Amount of carbon increased significantly in bio-char as compared to respective raw biomass (43.84 to 78.98 wt.%) while content of oxygen reduced from 48.79 to 18.11 wt.% when biomass was subjected to pyrolysis under different parametric conditions. The presence of high carbon content (in bio-char) confirms suitability towards bio-energy generation (Arif et al., 2021) and it is easy to ignite a fuel which has more oxygen content (Haykiri-Acma and Yaman, 2008). Thus, blend of carbon rich bio-char with oxygen and volatile matter rich biomass may prove to be useful for bio-energy production as bio-char will contribute to the calorific value while biomass will promote early ignition. At the same time minute and almost negligible amounts of nitrogen and sulfur in MAS-N, MAS-C and their bio-chars indicate very low emission of NO_X and SO_X by them. All these properties of MAS-N, MAS-C and their bio-chars make them suitable and significant source of bio-based energy, fuel and chemical generation.

Table 5.1. Characterization of MAS-N, MAS-C and their bio-chars

Property	MAS-N	MAS-C	BC-N	BC-450	BC-500	BC-550	BC-600
MC (wt.%)	6.64	6.1	5.4	4.1	3.6	2.8	2.2
VM (wt.%)	78.30	78.1	32.1	31.7	26.8	23.5	22.1
AC (wt.%)	2.04	4.6	5.92	6.9	7.4	8.5	9.5
FC (wt.%)	13.02	11.2	56.58	57.3	62.5	65.2	66.2
C (wt.%)	43.84	49.1	76.93	73.68	76.96	78.01	78.98
H (wt.%)	6.49	5.7	3.76	4.07	3.35	3.02	2.17
N (wt.%)	0.88	0.86	0.78	0.83	0.79	0.76	0.74
O (wt.%)	48.79	44.34	18.53	21.42	18.9	18.21	18.11
H/C	1.76	1.39	0.58	0.66	0.52	0.46	0.32
O/C	0.83	0.67	0.18	0.21	0.18	0.17	0.17
HHV (MJ/kg)	16.34	16.46	24.76	24.76	23.11	24.03	21.12

5.3.5 TG/DTG analysis of MAS-C and MAS-N

Thermogravimetric analysis (TGA) serves as an analytical technical tool for determining a sample's thermal stability, volatile fractions and thermal events associated with its decomposition by monitoring the weight change occurring at a constant heating rate. TG/DTG curves of a material impart its thermal decomposition profile as a function of temperature (Agnihotri et al., 2023). TG and DTG thermograms of non-catalytic (MAS-

N) and catalytic (MAS-C) biomass are illustrated in Fig. 5.4. TGA of MAS-N and MAS-C was carried at 10, 20 and 30 ℃/min heating rates under 100 mL/min purging of highly pure (99.99%) nitrogen gas from room temperature to a specified temperature of 800 ℃. Degradation of biomass can be classified into various regions or stages such as devolatilization of water, followed by lignocellulosic degradation, namely hemicellulose, cellulose and lignin decomposition (Font et al., 2005).

TG behavior of MAS-N is depicted in Fig. 5.4 (a), (b) and (c). For TG curves corresponding to 10 ℃/min, from ambient to 180 ℃ around 6% loss in mass was recorded and it relates to moisture-removal along with few light volatiles. About 62% mass loss was observed in second stage often called as active pyrolysis stage corresponding to 210-480 ℃. Decomposition of hemicellulose and cellulose occurred in this stage. Beyond 480 ℃ slight and gradual devolatilization took place with lignin degradation being the principal reaction in this stage. In this region charring also occurs and this pyrolysis zone is also referred to as passive pyrolysis stage. Lignin degradation occurred quite slowly over a broad temperature range of 180-800 ℃ due to polymorphism and absence of basic structure (Khan et al., 2016) and it is accountable for long tail in DTG curves. More or less similar degradation pattern in all three curves can be noticed regardless of whatever heating rate is employed.

DT/DTG plots at higher heating rates exhibited similar shapes which points out similar degradation mechanism, but DTG curves and its peaks (Fig. 5.4 (c), (d) and (e)) shifted towards higher temperature. This nature is ascribed to thermal lag arising due to uneven heating and corresponding heat transfer resistance at high heating rates. Low heating rates provide uniform and even heating of biomass (Loy et al., 2018). Higher heating

rates facilitate quick devolatilization and fragmentation by shortening reaction-time which in turn prevents repolymerization of volatiles (Da Silva et al., 2022).

Catalytic effect of Cu can be seen from TG/DTG curves secured for MAS-C at 10, 20 and 30 ℃/min (Fig. 5.4). Thermal degradation of MAS-C exhibited similar pattern as that of MAS-N. But TG curves shifted slightly downwards as depicted in Fig. 5.4 (a), (b) and (c) indicating lower decomposition temperature as a result of catalytic effect. Also, height of peaks of DTG plots (Fig. 5.4 (d), (e) and (f)) increased, intensified and became more pronounced for MAS-C as compared to that of MAS-N which signified enhancement in rate of reaction upon catalyst introduction. Similar results were announced for tobacco rob (Yang et al., 2011) and douglas fir (Wang et al., 2018a). Maximum mass loss rate corresponds to the stage of conversion where the depolymerization rate is the highest (Collard and blin, 2014). Maximum mass loss occurred at 365, 371 and 392 ℃ for MAS-N but it jumped down to 355, 357 and 338 ℃ corresponding to 10, 20 and 30 ℃/min, respectively for MAS-C. It indicates that both improvement in mass loss rate and reduction in the temperature of biomass thermal degradation was attained due to catalytic effects. Cu catalyst facilitated better heat transfer within the biomass. This could mainly be attributed to ability of metal catalyst to enhance the rate of cracking and reforming reactions (Yang et al., 2011). Similar trend of TG curves was reported for *Arundo donax* and *Broussonetia papyrifera* upon impregnation with heavy metals (Han et al., 2018). Maximum thermal decomposition temperature of poplar wood decreased from 373.9 to 359.0 ℃ due to potassium impregnation (Hwang et al., 2013). Thus, all these findings infer effectiveness of the catalytic effect imparted by Cu in bringing down energy requirement in pyrolysis by lowering temperature required for attaining a particular level of conversion.

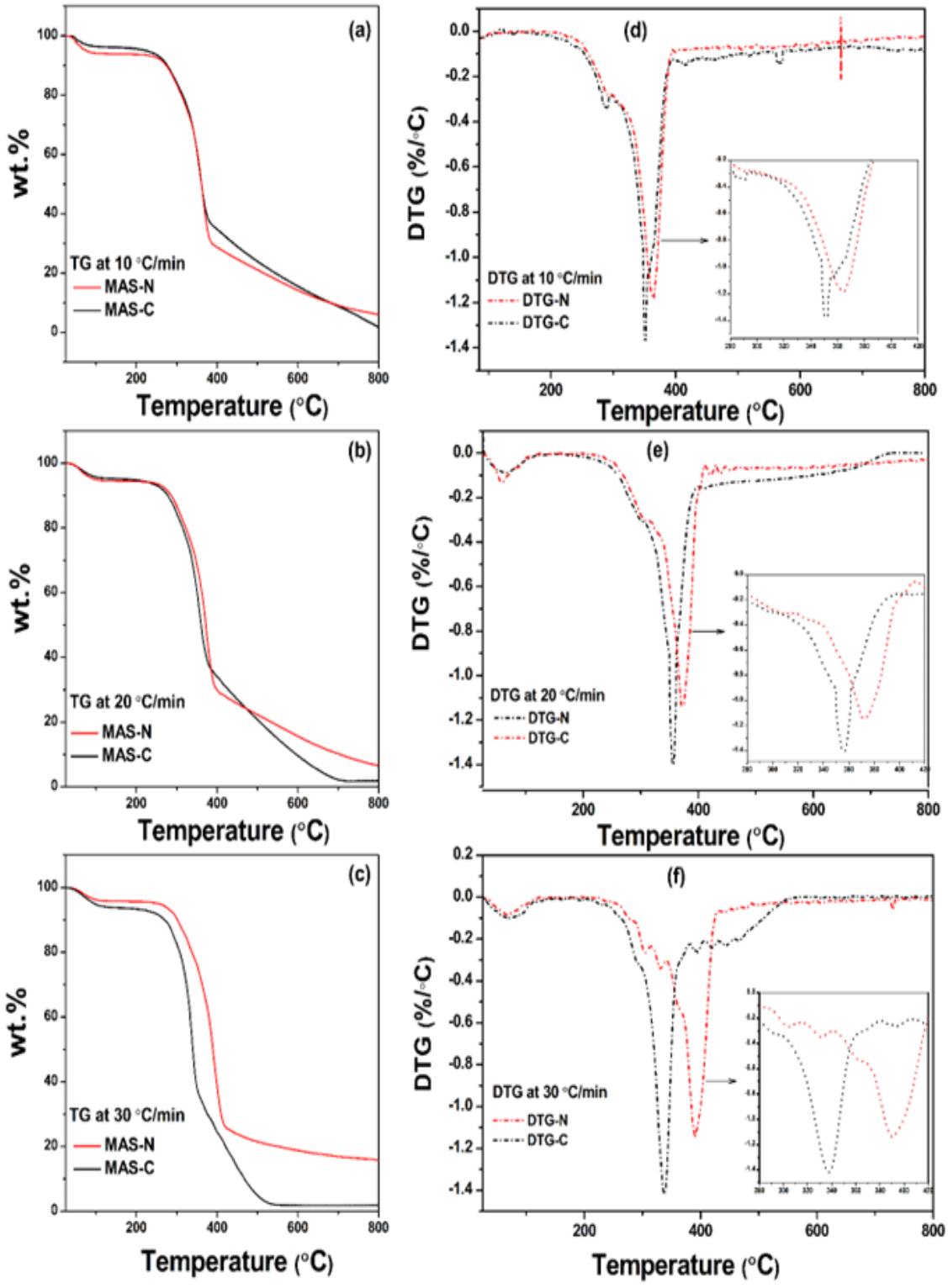

Figure 5.4. TG/DTG curves of MAS-N and MAS-C obtained at (a)/(d) 10 °C/min (b)/(e) 20 °C/min and (c)/(f) 30 °C/min

5.3.6 BET analysis of biomass and bio-char

Brunauer–Emmett–Teller (BET) method is a widely used characterization technique which aims at evaluating textural and surface properties of the material. BET surface area along with pore volume and mean pore size have been presented in Table 5.2. It is observed from the table that BET surface area of bio-chars of MAS-C increased when it was subjected to pyrolysis. Increase in BET surface area from 1.37 to 120.31 m^2/g was observed when pyrolysis temperature raised from 450 to 500 ℃. BET surface area of the bio-char is significantly influenced by the temperature of pyrolysis and it increased on increasing pyrolysis temperature up to 500 ℃ owing to the fact that liberation of more volatiles took place as temperature was elevated (Gupta et al., 2019). But on further increasing temperature to 600 ℃ BET surface area reduced to 91.46 m^2/g, this might be a result of collapsing, shrinking, merging of smaller pores into larger ones and sintering of some pores (Maruoka et al., 2018). Furthermore, it is worth noticing that BET surface area obtained for all bio-chars of MAS-C is less than that of BC-N (obtained by pyrolysis of MAS-N) because of blocking of some pores by metal particles and loading of metallic sites into the sawdust. Pore volume increased upon increasing pyrolysis temperature while decrease in mean size of pore was obtained with increasing pyrolyzing temperature but highest pore volume (0.159 cm^2/g) and lowest mean pore size (2.399 nm) was obtained for non-catalytic bio-char, that is, BC-N. Reason for this pattern of pore volume and mean pore diameter is introduction of metal particle species within the matrices due to impregnation. As per classification of IUPAC, bio-chars obtained in this study are mesoporous material because their pores size lie in the range of 2-50 nm. So, this mesoporous bio-char can find a wide variety of applications such as acting as a catalyst support, fine chemical synthesis, selective adsorption, chemical sensors (Kalita and

Kumar,2007) and cost-effective highly efficient metal-doping mesoporous graphite-like catalysts (Xu et al., 2022).

Table 5.2. Surface properties of MAS-C and biochar

Sample name	BET surface area (m^2 /g)	Pore volume (cm^3 /g)	Mean pore size (nm)
BC-N	240.2	0.159	2.399
MAS-C	1.37	0.009	29.584
BC-450	12.98	0.043	10.314
BC-500	120.31	0.091	3.0021
BC-550	99.7	0.078	3.0836
BC-600	91.46	0.078	3.0901

5.3.7 XRD analysis of MAS-N, MAS-C and bio-char

X-ray diffraction (XRD) is a characterization technique which finds its application in identification of crystallinity of any material. Pattern of XRD diffractograms for MAS-N, MAS-C and their bio-chars is presented in Fig. 5.5. Two intensified sharp peaks about 18 and 22^0 values of 2Θ are visible in diffractograms of MAS-N as well as in MAS-C and these peaks are assigned to cellulosic crystalline region owing to the fact that hemicellulose and lignin exhibit commonly amorphous nature. Diffractograms obtained for bio-chars showed less intense and broader peaks around 2Θ value of 22^0. This indicates decomposition of lignocellulosic structure during the course of pyrolysis.

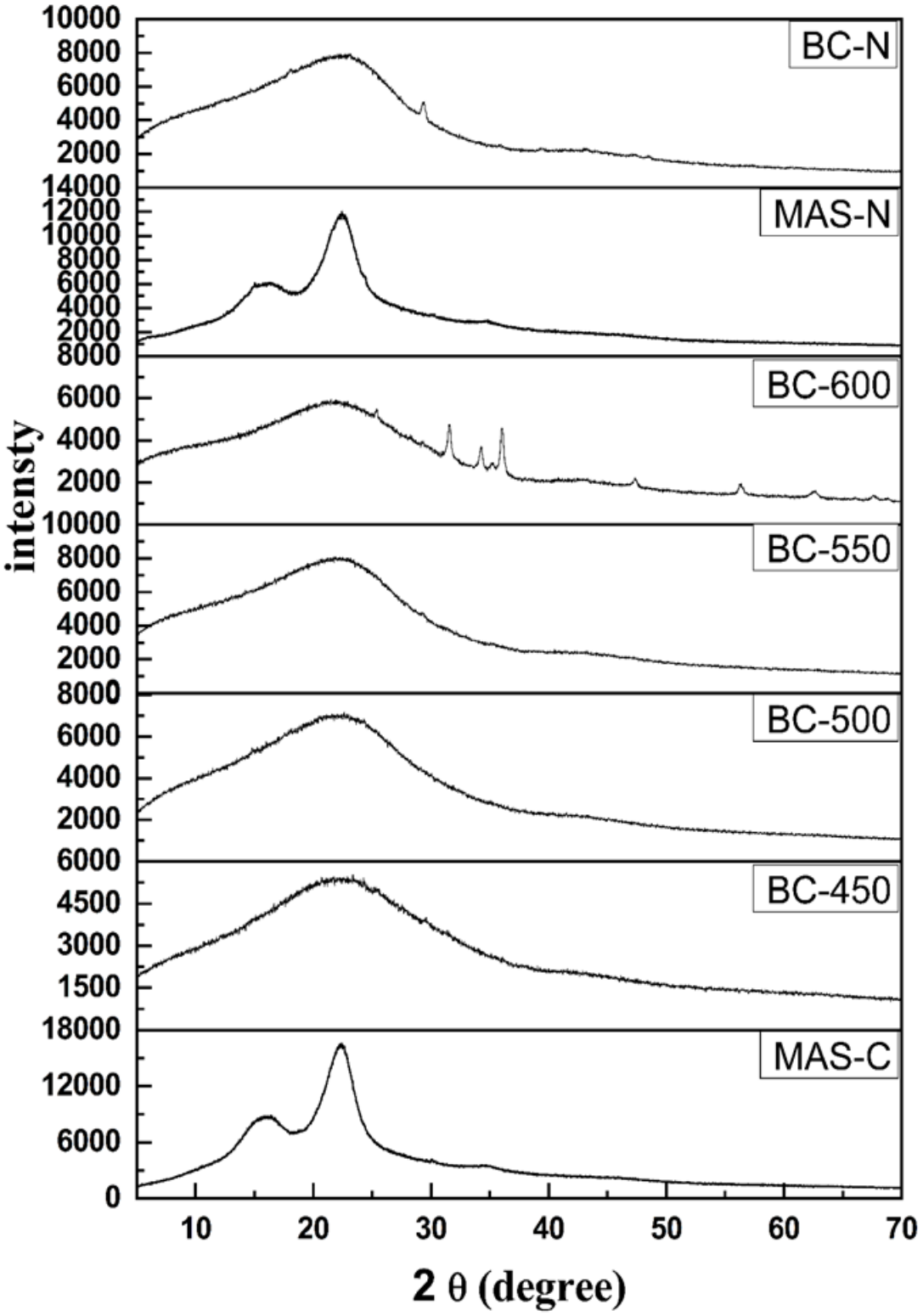

Figure 5.5. XRD analysis of MAS-N, MAS-C, and bio-char (150 mL/min N_2 flow rate, 0.18-0.29 mm particles, 8.4 cm bed height, 60 min pyrolysis time and 20 ℃/min heating rate)

It can be noticed from pattern of XRD peaks for biomass and bio-chars that upon catalytic treatment of MAS-N its cellulosic portion disintegrated and transformed into pyrolytic products as peaks in catalytic bio-chars portion disintegrated and transformed into pyrolytic products as peaks in catalytic bio-chars became broader and diminished. So, catalytic treatment by Cu impregnation provided better conversion in comparison to non-catalytic one. Due to catalytic pyrolysis crystalline characteristics of samples decreased and it acquired amorphous characteristics more.

5.3.8 FTIR analysis of MAS-N, MAS-C and bio-char

FTIR spectrum provides vibration stretches which serve as a fingerprint for identification of various functional groups of a substance. These vibration spectra have unique properties and impart unique characteristics to molecules. The FTIR spectra of MAS-N, MAS-C, BC-N, BC-450, BC-500, BC-550 and BC-600 is shown in Fig. 5.6. A broad peak around 3430 cm^{-1} in all the samples is present which is due to hydrogen-bonded O-H stretch of phenols and alcohols such as methanol which suggests presence of these groups in the samples. Intensity of these peaks reduced in catalytic bio-chars as compared to MAS-N, MAS-C and BC-N which indicated higher conversion of these compounds into some others due to catalytic effect. Peak at 2910 cm^{-1} in MAS-N and MAS-C samples indicates the existence of stretches of C-H vibrations arising due to saturated aliphatic groups and alkanes like methane. Stretching vibrations arising around 1740 cm^{-1} is an indicative of presence of C=O which relates to existence of aldehydes like ethanal, ketones like acetones and esters such as methyl formate. While these peaks disappeared in samples of bio-chars owing to the fact that these groups converted into the volatile fractions.

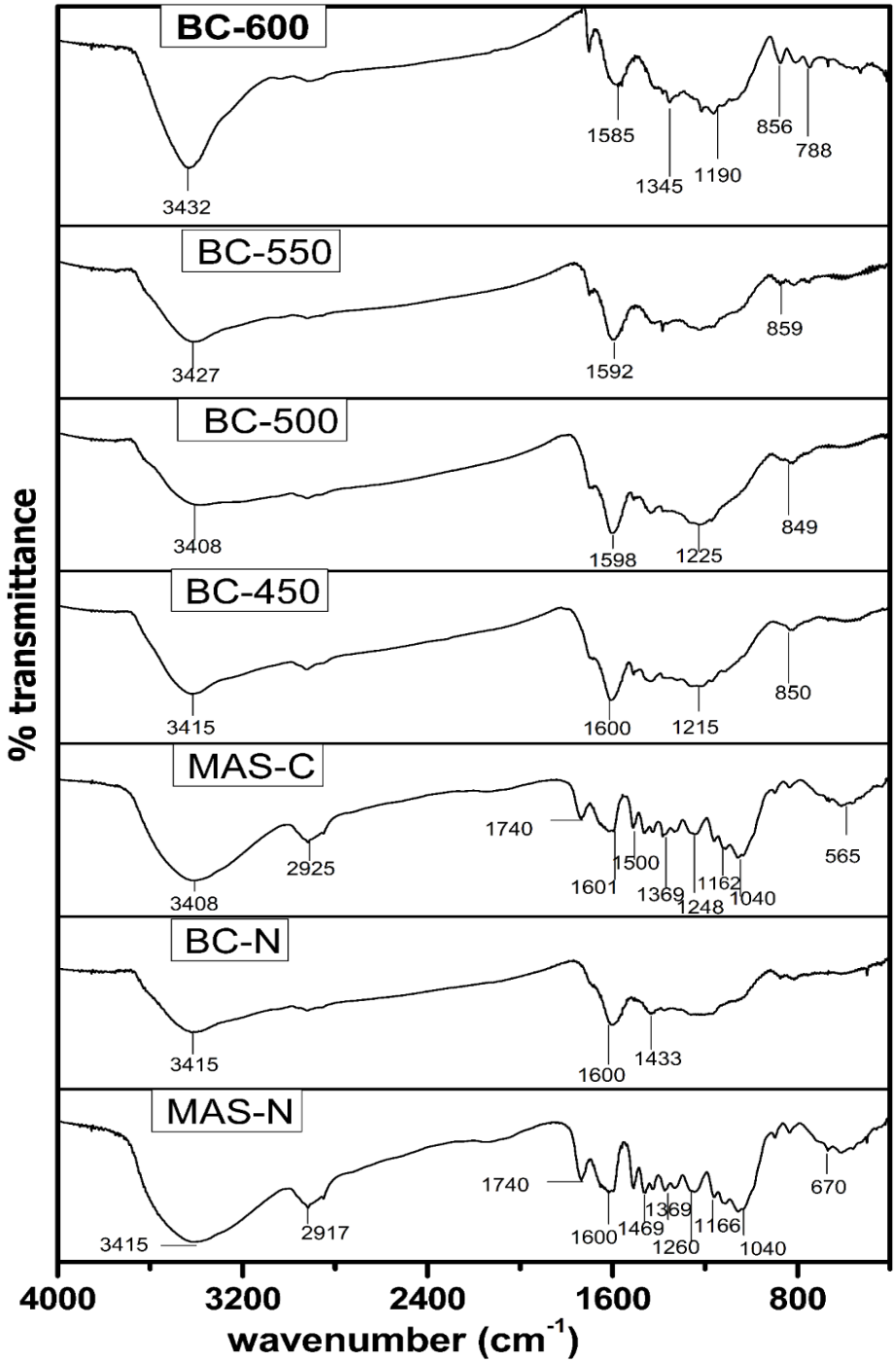

Figure 5.6. FTIR spectra of MAS-N, MAS-C and their bio-chars (150 mL/min N_2 flow rate, 0.18-0.29 mm particles, 8.4 cm bed height, 60 min pyrolysis time and 20 °C/min heating rate)

Peak existing around 1600 cm^{-1} relates to C−C=C vibrations of aromatic rings like benzene. Peak of 1510 cm^{-1} in substrate biomass affirms N=O stretch relating to the presence of nitro groups in it but its intensity decreased in MAS-C as compared to MAS-N because of catalytic effect imparted by Cu due to secondary reactions. A number of stretch bands are visible from 1040-1500 cm^{-1} in MAS-N and MAS-C which are testimony of C−O stretches of esters and ethers and eventually disappearance of these peaks in corresponding bio-chars emphasises their conversion on being subjected to pyrolysis. Vibrations of C−H stretching of monocyclic and polycyclic aromatic compounds are responsible for peaks occurring at 856 cm^{-1} in samples of catalytic bio-chars and these are absent in non-catalytic samples. A small peak near 550 cm^{-1} could be attributed to Cu and it indicates proper incorporation of the metal in the biomass (Pradeep and Chandrasekaran, 2006).

5.3.9 SEM-EDX analysis of MAS-N, MAS-C and bio-chars

SEM-EDX analysis was done to have an idea about morphological and textural characteristics of biomass and bio-char. Fig. 5.7 represent SEM-EDX images of MAS-N, BC-N, MAS-C and BC-500. Both MAS-N (Fig. 5.7a) as well as BC-N (Fig. 5.7b) possessed porous structure but surface area of bio-char got augmented as compared to that of MAS-N. This happened because volatile fractions of MAS-N released from biomass interstices due to high temperature resulting in higher number of pores coupled with enhanced internal specific surface area of pores. Spherical craters of MAS-N surface were transformed into open channel cells of BC-N post carbonization and devolatilization of volatile fractions from MAS-N. Rich porous morphology and enhanced specific surface area of bio-char is favourable as it makes bio-char efficient to be used in various applications such as soil conditioning, catalyst support, solid-liquid adsorption and waste water treatment substrate (Wang et al., 2022).

SEM micrographs of MAS-C and its bio-char, BC-500 (as shown in Fig. 5.7c and d), respectively) revealed that Cu metal got coated upon its surface. As a result of metal doping porous structure of biomass got distorted and upon pyrolyzing heavy metal loaded bio-char pore density enhanced but presence of metals in it is clearly visible from the image. This shows metallic portion remained in solid bio-char and did not volatilize with volatile fractions of sawdust.

Effect of heavy metal impregnation and their presence in corresponding bio-char is clearly visible from EDX pictures of MAS-C and BC-500 (Fig. 5.7e and f, respectively). Elemental mapping of MAS-C exhibited peaks of Cu, showing uptake of the metals on surface of biomass upon impregnation. Similarly, peaks of Cu in EDX image of BC-500 reflects these metals remained in the solid pyrolysis bio-char even after pyrolysis. So, at 500 ℃ temperature there is no possibility of secondary contamination or volatilization of the heavy metals into the bio-oil fraction. So, bio-oil free from heavy metals is obtained by pyrolyzing MAS-C at 500 ℃, this is particularly important for obtaining metal-free bio-oil from heavy metal contaminated plants resulting from phytoremediation.

Similar results were announced for heavy metal contaminated hardwood (Stals et al., 2010) and *sorghum bicolor* shoots resulting from phytoremediation (Chami et a., 2014). Kistler et al. (1987) reported Cr, Ni, Cu, Zn, and Pb completely retained in the solid residue of pyrolysis up to 750 ℃ (Kistler et al., 1987). Therefore, Cu-enriched bio-char can find its application in the preparation of functional materials like catalysts, adsorbents, capacitors, chemical reagents, antibacterial materials, soil additives, and supplying heat for the fast pyrolysis.

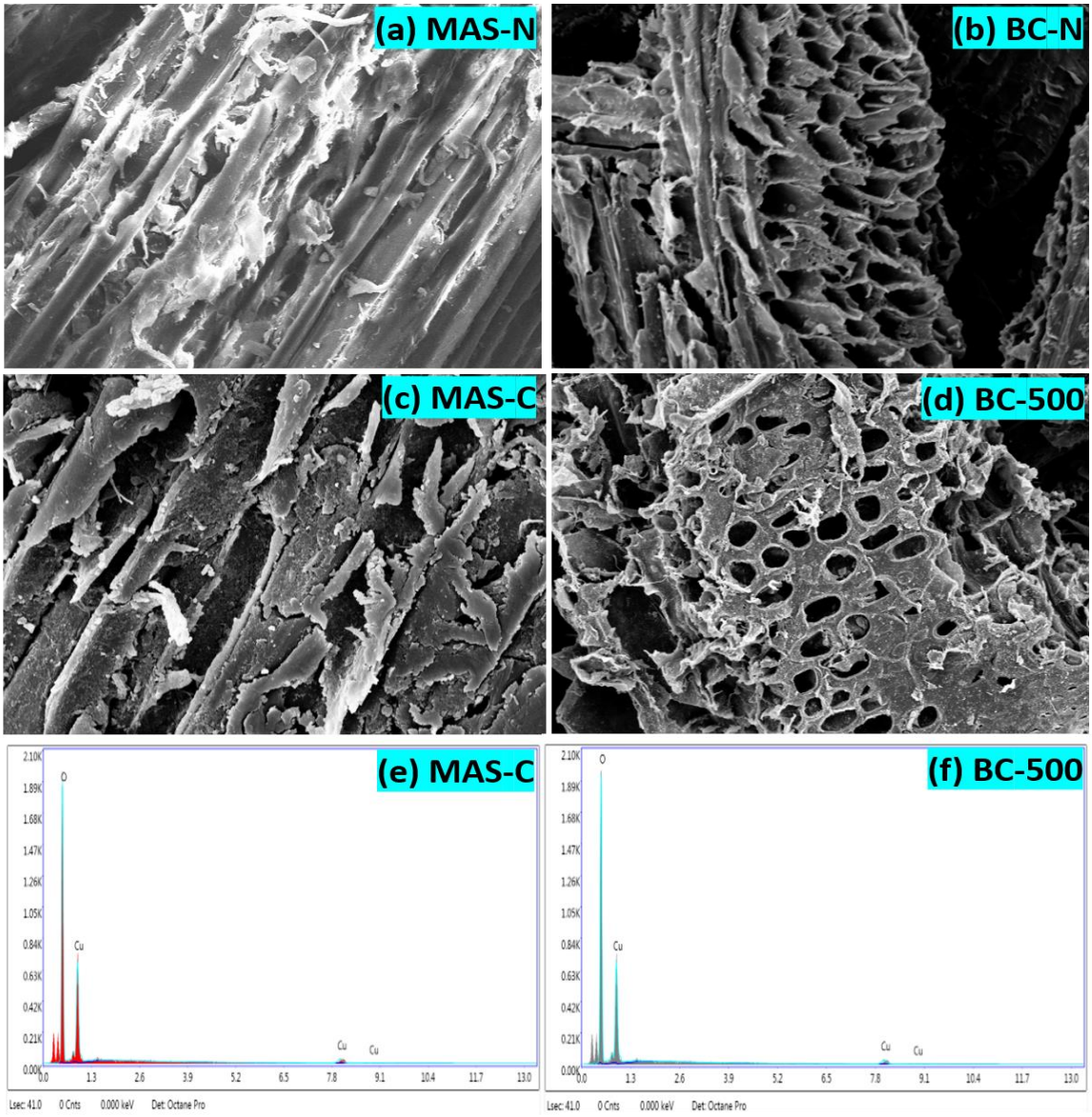

Figure 5.7. SEM-EDX images of MAS-N, MAS-C and bio-chars (150 mL/min N_2 flow rate, 0.18-0.29 mm particles, 8.4 cm bed height, 60 min pyrolysis time and 20 ℃/min heating rate)

5.3.10 FTIR analysis of non-catalytic and catalytic bio-oil

Spectrum obtained for FTIR analysis of non-catalytic (BO-N) and catalytic bio-oils (obtained at 450, 500, 550 and 600 ℃) is presented in Fig. 5.8. Vibration spectra of FTIR serve as fingerprint corresponding to various functional groups of the sample. A wide peak of hydrogen-bonded O-H stretch between 3600-3100 cm^{-1} is observed in all the

samples and it confirms availability of phenols and alcohols in these samples. It is less sharp for non-catalytic bio-oil than catalytic bio-oil suggesting difference in quantities of these compounds in both type of samples. Vibration peaks at 2965 and 2901 cm^{-1} infer presence of saturated aliphatic hydrocarbons or alkanes. Stretching vibrations of C=O is presented by band between 1730-1650 cm^{-1} in non-catalytic bio-oil which indicates carboxylic acid while in case of catalytic bio-oils peaks are found to occur around 1635 cm^{-1} which relates to C=O vibrating stretches of ketones and aldehydes. It can be concluded from this observation that upon introduction of catalyst acidity of bio-oil reduced. A sharp peak at 1570 cm^{-1} in non-catalytic bio-oil sample marked the existence of N=O stretch of nitrogenous compounds in it while no such peaks were present in FTIR spectra of catalytic bio-oil samples. A large number of vibration peaks can be seen arising from 1300 to 1000 cm^{-1} indicating C-O stretches related to easters and ethers in the sample. Vibrations of C-H related to polycyclic and monocyclic aromatic compounds is confirmed by the presence of peaks around 650 cm^{-1} and these peaks got intensified in case of catalytic bio-oil samples as compared to that of non-catalytic one. This could be attributed to the presence of Cu in wastewater used as catalyst in this study, which caused thermal degradation of lignin content into small molecular aromatic compounds. Similar result was reported for fir sawdust upon using Cu contaminated effluent as catalyst (Bhattacharjee and Biswas, 2019). It is clear from the Fig. 5.8 that intensity of stretching vibrations C=O, C-O and N=O diminished significantly in FTIR spectra of catalytic bio-oil as compared to that of non-catalytic bio-oil sample meanwhile C-H stretches related to aromatic and aliphatic hydrocarbons acquired intensified peaks for catalytic bio-oil samples. It suggests transformation of oxygenated compounds associated with ketones, aldehydes, esters, ethers and carboxylic acid into hydrocarbons as a result of introduction of catalyst.

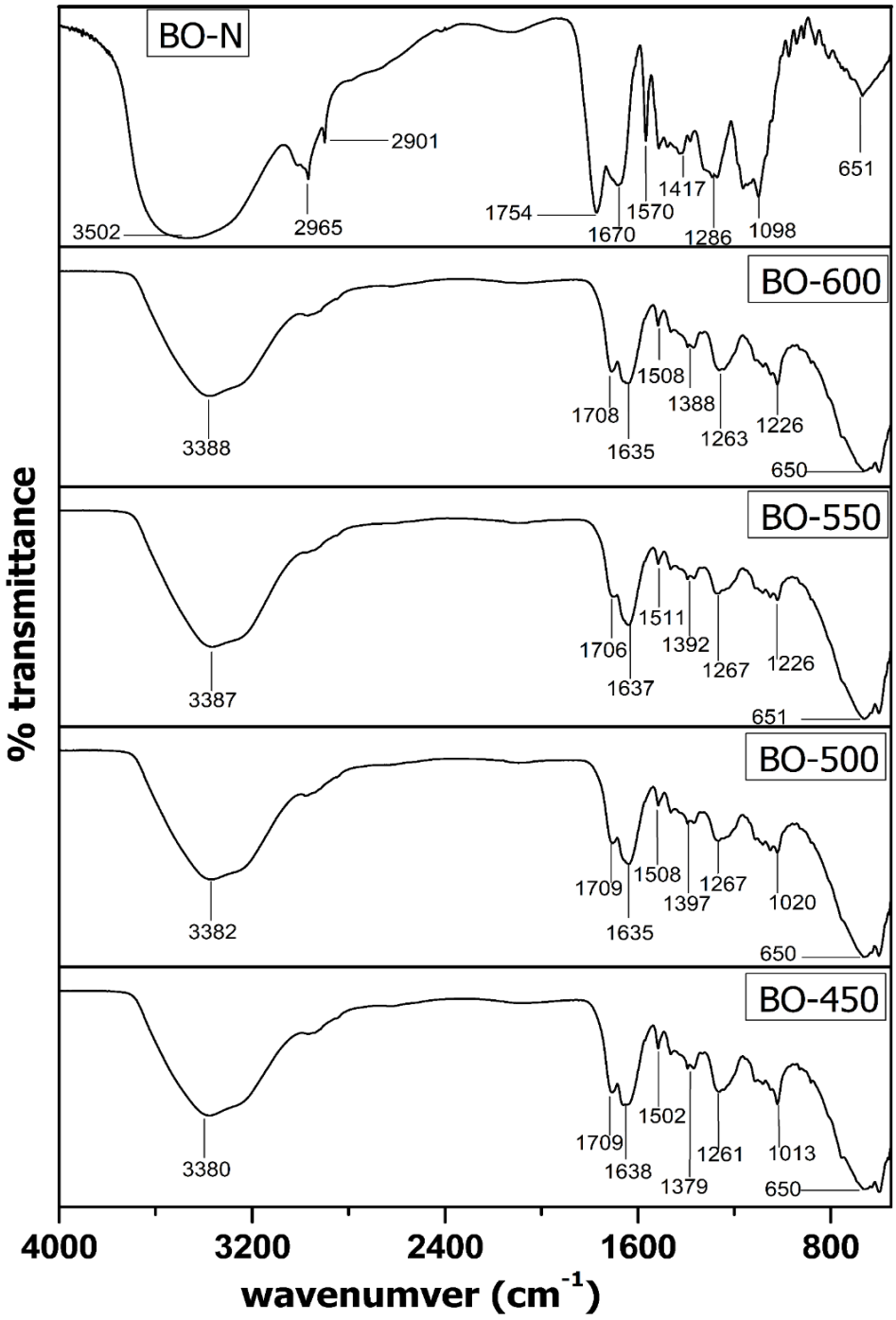

Figure 5.8. FTIR spectra of catalytic and non-catalytic bio-oils (150 mL/min N_2 flow rate, 0.18-0.29 mm particles, 8.4 cm bed height, 60 min pyrolysis time and 20 ℃/min heating rate)

5.3.11 ^{13}C NMR study of bio-oil

Identification of molecular composition of pyrolysis bio-oil is a tedious job as it consists

of a large number of chemical compounds. Nuclear magnetic resonance (NMR) is a prominent characterization technique for determination of various functional groups of pyrolytic bio-oil. ^{13}C NMR spectra was broadly categoried into five chemical shift regions as hydrocarbons (0-54 ppm), methoxy/hydroxy (54-70 ppm), carbohydrate (70-103 ppm), aromatic (103-163 ppm) and carbonyl carbon environment (163-215 ppm) (Kistler et al., 1987). Spectra for ^{13}C NMR analysis of bio-oils is portrayed in Fig. 5.9 and 5.10 (non-catalytic and catalytic, respectively). Existence of numerous functional groups such as alkyl hydrocarbons, methoxy/hydroxy, carbohydrate, aromatic and carbonyl carbon environment is confirmed by peaks in both non-catalytic and catalytic bio-oils. At 39.5 ppm strong peak of solvent deuterated DMSO-d_6 (dimethyl sulfoxide-d_6) was recorded in both the bio-oil samples. In range of 0–54 ppm several peaks with varying intensities are present in both type of bio-oils, number of peaks and intensity of few peaks increased in catalytic sample which may be due to increase in aliphatic carbons in it. In 70-103 ppm, more peaks were present in catalytic sample, suggesting more quantity of ethers, alcohols, phenolic-methoxy, and carbohydrate sugars in catalytic bio-oil than non-catalytic. In the region of 103-163 ppm, scattered peaks are present which got somewhat intensified for catalytic bio-oil. Aromatics in bio-oil are desired for bio-oil synthetic modification (Khuenkaeo et al., 2021). In 163-215 ppm few small peaks are present in both type of bio-oils, indicating presence of the carbonyl carbon groups (ketones and aldehyde) in less quantity. More peaks were present in carbohydrate, aromatic and carbonyl carbon region of the spectrum for catalytic bio-oil as compared to non-catalytic bio-oil. This indicated more production of these compounds as a result of catalyst introduction. Also, ^{13}C NMR spectra for both type of bio-oils exhibited more peaks for methoxy/hydroxy than hydrocarbons.

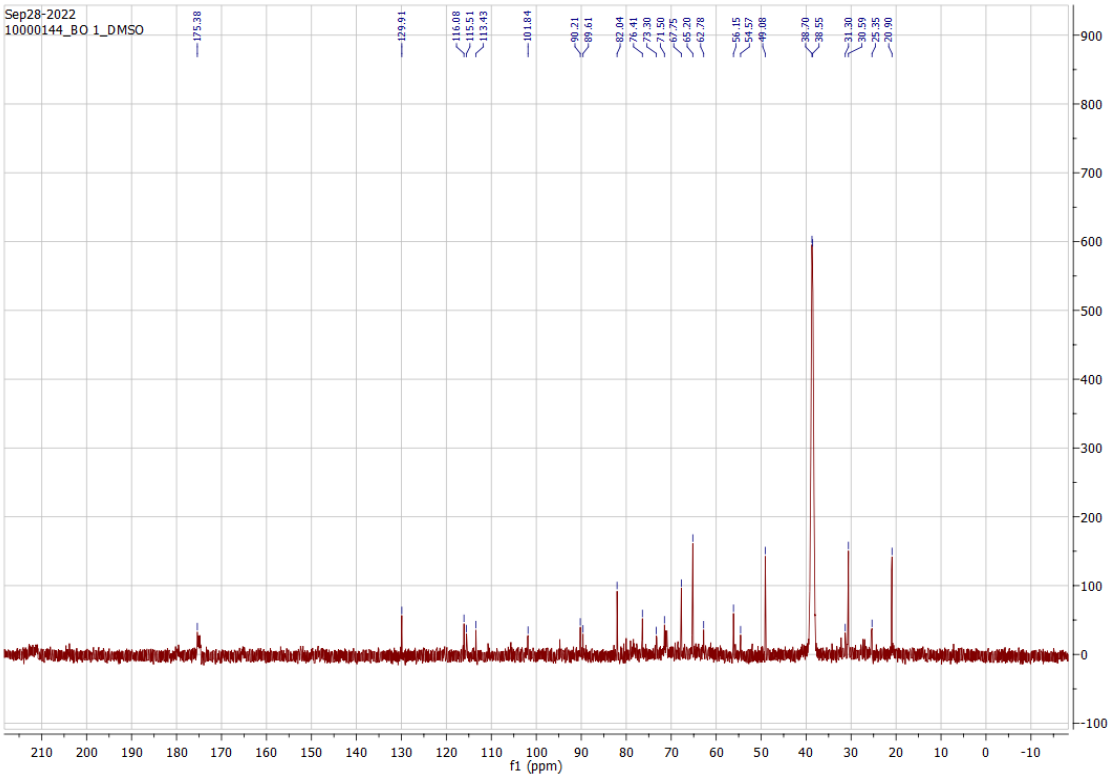

Figure 5.9. ^{13}C NMR Spectra of non-catalytic bio-oil (550 ℃ temperature, 150 mL/min N_2 flow rate, 0.18-0.29 mm particles, 8.4 cm bed height, 60 min pyrolysis time and 20 ℃/min heating rate)

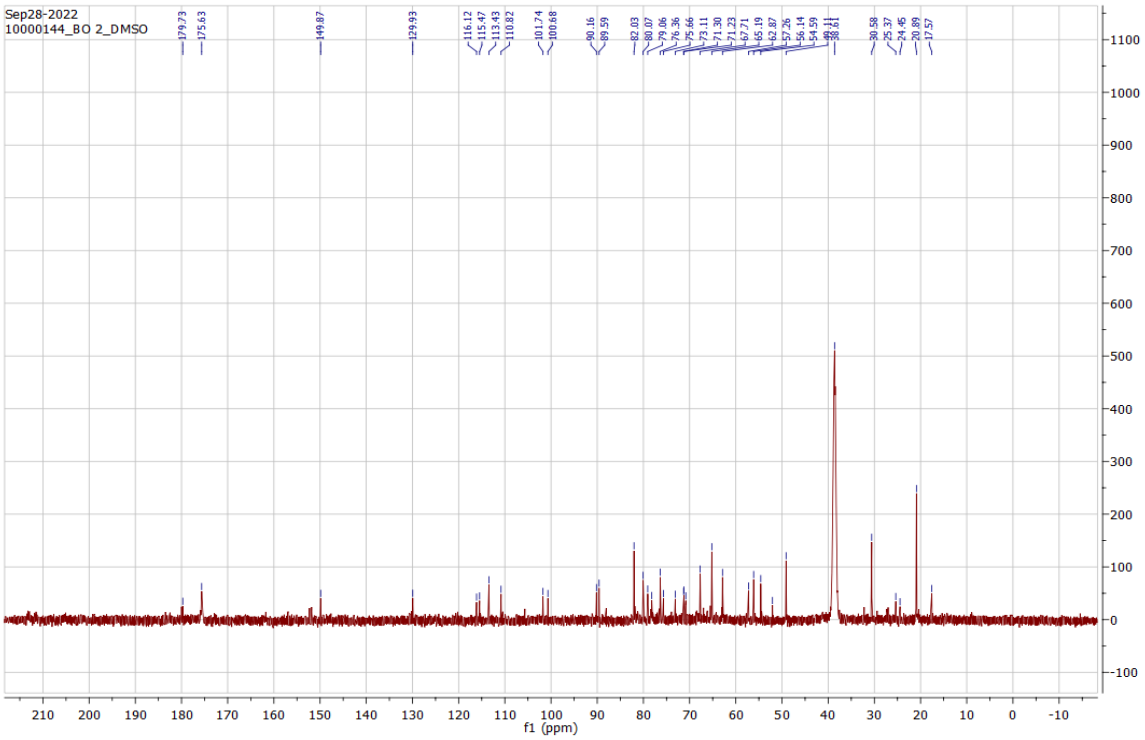

Figure 5.10. ^{13}C NMR Spectra of catalytic bio-oil (500 ℃ temperature, 150 mL/min N_2 flow rate, 0.18-0.29 mm particles, 8.4 cm bed height, 60 min pyrolysis time and 20 ℃/min heating rate)

5.3.12 GC–MS analysis of catalytic and non-catalytic bio-oils

GC-MS analysis gives information about varieties of constituent compounds existing in bio-oil. Table 5.3, 5.4 and Fig. 5.11, 5.12 illustrated that a variety of chemical compounds (in % of area) like phenols, furans, ketones, aldehydes, acids, alcohols, ester and sugar derivatives along with some other chemical compounds are present in bio-oils obtained at their optimum conditions (MAS-C at 500 ℃ and MAS-N at 550 ℃). Phenolic content was found to be 17.12 and 14.8 % for catalytic and non-catalytic bio-oils, respectively and main phenolic compounds detected (in MAS-C) were phenol, Phenol, 4-methoxy-3-(methoxymethyl)-, Phenol, 2,6-dimethoxy-, Phenol, 2-methyl- and 2-Methoxy-5-methylphenol. Formation of phenols mainly occurred due to the degradation of lignin content of biomass. This enhancement in phenolic content in catalytic bio-oil was observed because introduction of Cu catalyst promotes phenolic compounds via dehydration and demethylation reactions (Zheng et al., 2021). Aldehydes and ketones contributed 7.21 and 8.28%, respectively in catalytic bio-oil while non-catalytic bio-oil contained aldehydes and ketones 8.74 ad 16.3%, respectively. Catalytic bio-oil carried 16.83% furan derivatives and furans are a key starting material for production of agrochemicals, pharmaceuticals, resin, and lacquers (Khan et al., 2021). Chai et al. (2022b) produced 2, 5-furan dicarboxylic acid to replace petroleum-based terephthalic acid using contaminated biomass (Chai et al., 2022b). Catalytic bio-oil contained 3.65% while non-catalytic bio-oil 0.42% of hydrocarbons and 10.59% (in MAS-C) and 4.76% (in MAS-N) esters. In catalytic bio-oil sugar and alcohols contents were 12.51 and 9.52%, respectively. In non-catalytic bio-oil alcohols contributed 15.91%. Cu imparted its catalytic effects and reduced the oxygen content of the bio-oil along with enrichment in hydrocarbons and phenolic content in catalytic bio-oil. Therefore, bio-oil obtained by catalytic pyrolysis using Cu as catalyst

can be considered as an excellent source for production of bio-fuel and bio-based chemicals.

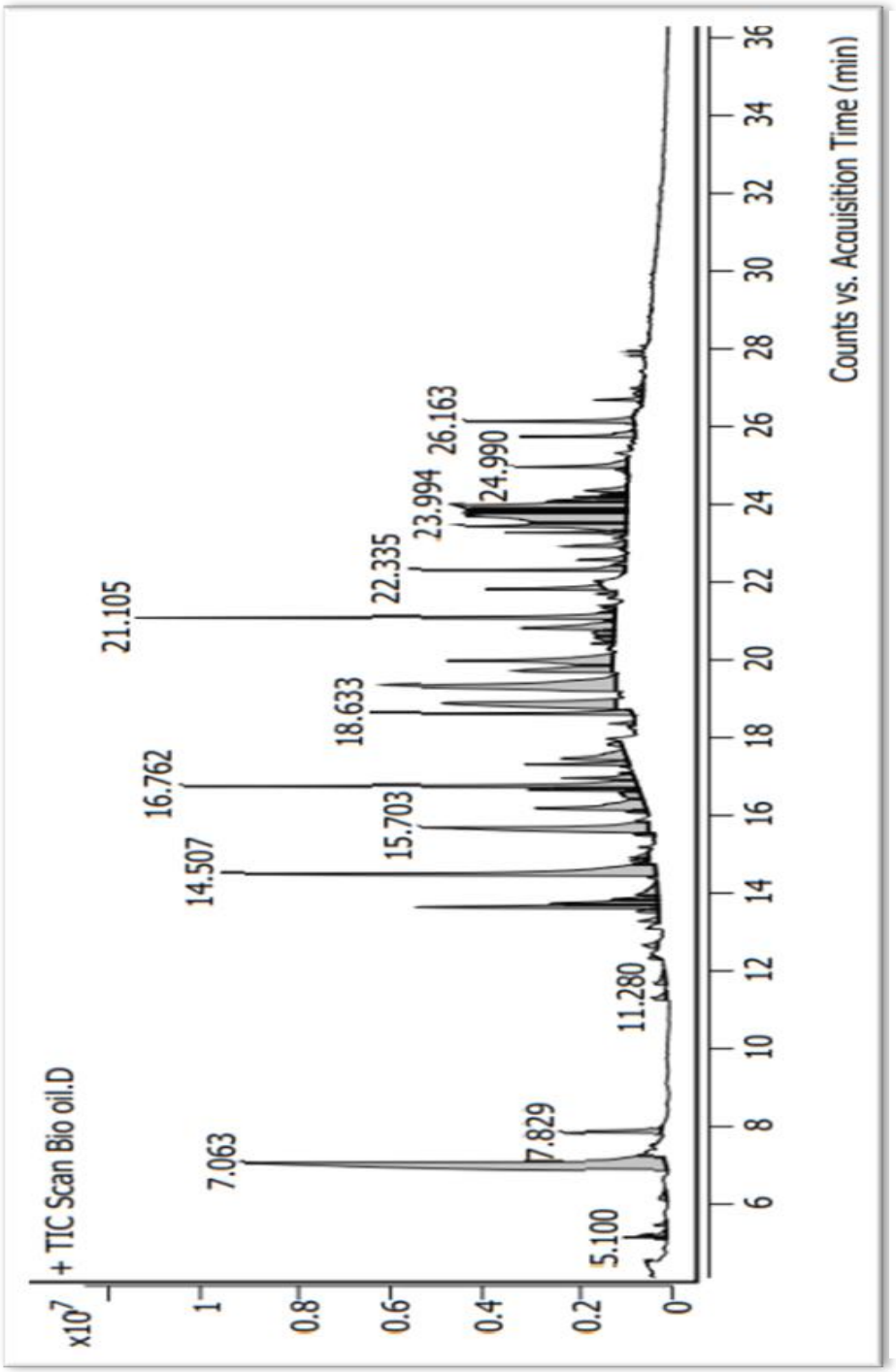

Figure 5.11. GC-MS chromatograph of catalytic bio-oil obtained at 500 °C (500 °C temperature, 150 mL/min N_2 flow rate, 0.18-0.29 mm particles, 8.4 cm bed height, 60 min pyrolysis time and 20 °C/min heating rate)

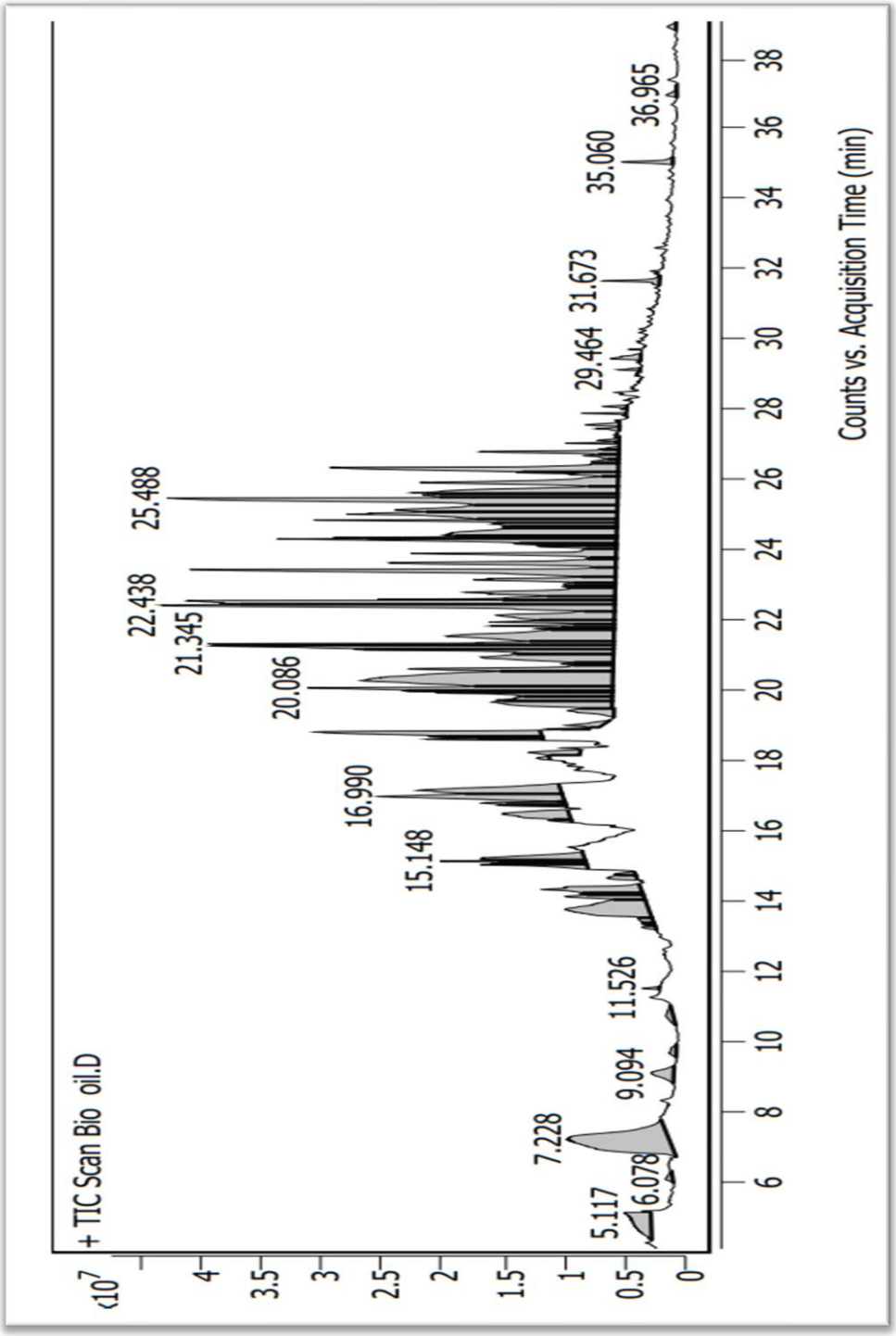

Figure 5.12. GC-MS chromatograph of non-catalytic bio-oil obtained at 550 °C (550 °C temperature, 150 mL/min N_2 flow rate, 0.18-0.29 mm particles, 8.4 cm bed height, 60 min pyrolysis time and 20 °C/min heating rate)

Table 5.3. GC-MS analysis of catalytic bio-oil obtained at 500 ℃

Retention time (min)	Compound Name	Molecular formula	Area %
5.100	Methyl propionate	$C_4H_8O_2$	0.32
5.449	1-Butene, 2,3,3-trimethyl	C_7H_{14}	0.13
6.12	3,4-Octadiene, 2,2-dimethyl	$C_{10}H_{18}$	0.2
7.06	3-Furaldehyde	$C_5H_4O_2$	12.38
7.829	Ethanol, pentamethyl-	$C_7H_{16}O$	1.20
11.280	4,5-Nonadiene	C_9H_{16}	0.29
13.740	2-Furancarboxaldehyde, 5-methyl-	$C_6H_6O_2$	2.93
13.740	2-Furancarboxaldehyde, 5-methyl-	$C_6H_6O_2$	1.52
13.855	4-Octyne	C_8H_{14}	0.56
13.975	Methyl 13,14-octadecadienoate or 13,14-18:2	$C_{19}H_{34}O_2$	0.59
14.507	Phenol	C_6H_6O	6.87
15.703	2H-Pyran-2-carboxaldehyde, 3,4-dihydro	$C_6H_8O_2$	4.62
16.201	3,4-Octadiene, 2,2,7,7-tetramethyl	$C_{12}H_{22}$	2.47
16.596	Methyl 12,13-tetradecadienoate	$C_{15}H_{26}O_2$	0.55
16.676	Phenol, 2-methyl-	C_7H_8O	1.35

16.762	2-Cyclohexen-1-one,4,4-dimethyl	$C_8H_{12}O$	4.8
16.973	Methyl 12,13-tetradecadienoate	$C_{15}H_{26}O_2$	0.75
17.328	2,3-Pentadienoic acid-,ethyl ester	$C_7H_{10}O_2$	1
17.471	Cyclohexanone, 4-ethyl	$C_8H_{14}O$	1.38
18.633	2-Methoxy-5-methylphenol	$C_8H_{10}O_2$	2.17
18.902	Ethylene diacrylate	$C_8H_{10}O_4$	4.29
19.336	Bicyclo[2.2.2]octane 1,4-diol	$C_8H_{14}O_2$	6.48
19.994	2-Nonynoic acid, methyl ester	$C_{10}H_{16}O_2$	3.09
20.721	2-Ethylnon-1-en-3-ol	$C_{11}H_{22}O$	0.45
20.841	2-Azido-2,4,4,6,6,8,8-heptamethylnonane	$C_{16}H_{33}N_3$	1.73
21.105	Phenol, 2,6-dimethoxy-	$C_8H_{10}O_3$	4.14
21.345	Phenol, 3,5-dimethoxy-	$C_8H_{10}O_3$	0.13
21.723	Undecanal	$C_{11}H_{22}O$	0.18
21.843	Phosphinic acid, diisopropyl-, menthyl ester	$C_{16}H_{33}O_2P$	1.21
22.335	Phenol, 4-methoxy-3-(methoxymethyl)-	$C_9H_{12}O_3$	1.66
22.941	1,4-Dimethoxy-2,3-dimethylbenzene	$C_{10}H_{14}O_2$	0.79
23.302	4-Ethyl-2,6-dimethoxyphenol	$C_{10}H_{14}O_3$	0.8

23.462	9-Thiabicyclo[3.3.1]non-2-en-6-amine, 9,9-dioxo-N-methyl-	$C_9H_{15}NO_2S$	2.86
23.771	D-Allose	$C_6H_{12}O_6$	5.82
23.834	3,4-Altrosan	$C_6H_{10}O_5$	1.39
23.897	.beta.-D Glucopyranose, 1,6-anhydro	$C_6H_{10}O_5$	1.41
23.994	1,6-Anhydro-.beta.-d talopyranose	$C_6H_{10}O_5$	4.22
24.109	Melezitose	$C_{18}H_{32}O_{16}$	1.06
24.990	Benzaldehyde, 4-hydroxy-3,5-dimethoxy	$C_9H_{10}O_4$	1.28
25.774	Benzaldehyde, 2,4,5-trimethoxy-	$C_{10}H_{12}O_4$	1.13
26.163	Syringylacetone	$C_{11}H_{14}O_4$	1.6
26.718	9H-Xanthene	$C_{13}H_{10}O$	0.45
27.015	Spiro[4.5]decan-7-one,1,8-dimethyl-8,9-epoxy4-isopropyl	$C_{15}H_{24}O_2$	0.15

Table 5.4. GC-MS analysis of non-catalytic bio-oil obtained at 550 ℃

Retention time (min)	Compound Name	Molecular formula	Area %
6.078	2-Furanmethanediol, dipropionate	$C_{11}H_{14}O_5$	6.078
7.228	Furfural	$C_5H_4O_2$	4.16
9.094	1,2-Nonadiene	C_9H_{16}	0.42
13.769	2-Azido-2,4,4,6,6- pentamethylheptane	$C_{12}H_{25}N_3$	2.19
15.148	Phenol	C_6H_6O	0.67
15.222	2-Vinylfuran	C_6H_6O	1.01
16.739	Bicyclo[2.1.0]pentane5-carboxylic acid, 1-methyl-, ethyl ester	$C_9H_{14}O_2$	0.25
16.801	2-Cyclohexen-1-one,4,4-dimethyl	$C_8H_{12}O$	0.4
16.99	5-Ethyl-2-furaldehyde C7H8O2	$C_7H_8O_2$	1.83
17.162	Benzyl alcohol	C_7H_8O	1.8
18.232	Phenol, 3,5-dimethyl-	$C_8H_{10}O$	0.39
18.621	3,3-Dimethyl-hepta-4,5-dien-2-one	$C_9H_{14}O$	0.43
18.695	3,3-Dimethyl-hepta-4,5-dien-2-one	$C_9H_{14}O$	0.38
18.827	2-Methoxy-5-methylphenol	$C_8H_{10}O_2$	1.93
18.919	2-Azido-2,4,4,6,6,8,8-heptamethylnonane	$C_{16}H_{33}N_3$	0.09

19.016	4H,5H-Pyrano[4,3-d]-1,3-dioxin, tetrahydro8a-methyl	$C_8H_{14}O_3$	0.27
19.434	Bicyclo[2.2.2]octane1,4-diol	$C_8H_{14}O_2$	0.47
19.68	Methyl 12,13-octadecadienoate	$C_{19}H_{34}O_2$	1.43
19.743	trans-(2-Ethylcyclopentyl)methyl acetate	$C_{10}H_{18}O_2$	0.94
19.937	Cyclohexanone, 2-(hydroxymethyl)-	$C_7H_{12}O_2$	1.01
20	2-Nonynoic acid, methylester	$C_{10}H_{16}O_2$	0.81
20.086	1-Cyclohexene-1-carboxaldehyde, 2,6,6-trimethyl	$C_{10}H_{16}O$	2.04
20.313	Cyclohexanone, 2-isopropyl-2,5-dimethyl	$C_{11}H_{20}O$	6.24
20.624	Y Methylbicyclo(4.3.0)non-6-en-8-one	$C_{10}H_{14}O$	1.43
20.961	Benzenemethanol, 4-hydroxy	$C_7H_8O_2$	1.76
21.179	Spiro[2.2]pentane-1- carboxylic acid, 2-cyclopropyl-2-methyl	$C_{10}H_{14}O_2$	1.6
21.282	Phenol, 2,6-dimethoxy-	$C_8H_{10}O_3$	2.84
21.345	2,4-Dimethoxyphenol	$C_8H_{10}O_3$	1.91
21.556	Cyclopentanepropanoic acid, 2-oxo-, methyl ester	$C_9H_{14}O_3$	2.83
21.848	2,7-Nonadienoic acid, 4,8-dimethyl-, methyl	$C_{12}H_{20}O_2$	0.56

	ester		
21.957	Benzene, 2,5-cyclohexadien-1-yl-	$C_{12}H_{12}$	0.68
22.152	Benzenethiol, 4-(1,1- dimethylethyl)-	$C_{10}H_{14}S$	1.58
22.438	6-Chromanol, methyl ether	$C_{10}H_{12}O_2$	3.39
22.564	3,5-Dimethoxy-4- hydroxytoluene	$C_9H_{12}O_3$	3.39
22.609	2,3-Dimethoxybenzyl alcohol	$C_9H_{12}O_3$	1.01
22.804	3-Isopropyl-1,2-benzenediol	$C_9H_{12}O_2$	1.6
23.164	p-Cymene-2,5-diol	$C_{10}H_{14}O_2$	1.1
23.456	4-Ethyl-2,6- dimethoxyphenol	$C_{10}H_{14}O_3$	3.3
23.645	Undeca-3,4-diene-2,10-dione	$C_{11}H_{16}O_2$	1.79
23.914	3-tert-Butyl-4- hydroxyanisole	$C_{11}H_{16}O_2$	1.39
24.114	Undeca-3,4-diene-2,10-dione, 5,6,6-trimethyl	$C_{14}H_{22}O_2$	0.4
24.189	2-Buten-1-one, 1-(2,2,5atrimethylperhydro-1-benzoxiren-1-yl)	$C_{13}H_{20}O_2$	0.46
24.326	2-Hydroxy-4-isopropyl7-methoxytropone	$C_{11}H_{14}O_3$	2.07
24.366	2,6-Dimethoxy-4-propylphenol	$C_{11}H_{16}O_3$	1.2

5.4 Conclusions

Non-catalytic and catalytic pyrolysis of MAS-N was carried out using Cu metal as catalyst. Results revealed that Cu had certain catalytic effect on yield and properties of pyrolytic products. This study demonstrated possibility of reducing secondary environmental pollution and provides a low-cost and sustainable solution for the preparation of functional materials like catalysts, adsorbents, capacitors, antibacterial materials, soil additives, and chemical reagents. This study demonstrated new pathway of safe treatment, disposal and value-added utilization of heavy-metal contaminated waste biomass. Cu acted as a catalyst and decreased temperature requirement for degradation of MAS-C (maximum bio-oil yield was obtained at 500 ℃ for MAS-C while that for MAS-N was obtained at 550 ℃) and also enhanced rate of reaction as compared to that of MAS-N. Cu impregnation also reinforced production of carbohydrate, aromatic and carbonyl groups in bio-oil. Several key differences in the product yield of bio-oils obtained from non-catalytic and catalytic process were noticed. Like upon introduction of catalyst acidity of the bio-oil reduced as compared to bio-oil obtained from non-catalytic pyrolysis. FTIR results also affirmed enhancement of aromatic compounds in catalytic bio-oil and transformation of oxygenated compounds associated with ketones, aldehydes, esters, ethers and carboxylic acid into hydrocarbons as a result of introduction of catalyst took place. Results of NMR spectra indicated increase in aliphatic carbon in catalytic bio-oil sample. Increment in the quantity of ethers, alcohols, phenolic methoxy, and carbohydrate sugars in catalytic bio-oil was observed as compared to that for non-catalytic bio-oil. GC-MS results revealed that because of catalytic effect of Cu, enhancement of phenolic and hydrocarbon content along with the reduction in oxygen content in the catalytic bio-oil in comparison to non-catalytic bio-oil.

So, pyrolysis of heavy metal contaminated biomass provides safe disposal approach for waste biomass, heavy metal polluted wastewater and biomass from phytoremediation. Therefore, Value-added conversion via pyrolysis of biomass provides new opportunities for energy generation, curbing heavy metal pollution, and the safe treatment of heavy metal polluted biomass resources.